Materials Research. 2021; 24(suppl 2): e20220049
DOI: https://doi.org/10.1590/1980-5373-MR-2022-0049

Evaluation Through SEM Image Processing of the Volumetric Fiber Content in Continuos Fiber-Reinforced Additive Manufacturing Composites

J. G. Díaz[a], *J. León-Becerra*[a], *A. D. Pertuz*[b], *O. A. González-Estrada*[a], *M. I. Jaramillo-Gutiérrez*[c]

[a]*Universidad Industrial de Santander, Escuela de Ingeniería Mecánica, Cra 27 Calle 9, Bucaramanga, Colombia.*
[b]*Universidad Industrial de Santander, Escuela de Ingeniería Mecánica, Grupo de Investigaciones en Corrosión (GIC), Cra 27 Calle 9, Bucaramanga, Colombia.*
[c]*Servicio Nacional de Aprendizaje (SENA), Centro Industrial del Diseño y la Manufactura (CIDM), Tecnoparque Nodo Bucaramanga, Grupo de Investigación EINSTEIN, Calle 40 #28-40, Bucaramanga, Colombia.*

Received: February 01, 2022; Revised: March 29, 2022; Accepted: March 31, 2022

This work shows the estimation of the volumetric fiber content (Vf) using image processing techniques. The Vf is needed to establish mechanical properties of composites using the rule of mixtures or other more advanced prediction models for the mechanical properties. The proposed method is tested with images acquired for carbon, Kevlar, and fiberglass fiber bundles used in the fiber deposition modeling (FDM) in the additive manufacturing process. The fiber bundles are provided by Markforged ® and are used in the Markforged Two ® printer. Then, different gray threshold and segregation algorithms are convolved with the digitized images to to isolate matrix from fibers such that a separate fiber and matrix area counting can be done and an appropriate Vf can be established. Results obtained with image analysis are close to values reported using technical standards, hence validating the proposed method.

Keywords: *Fiber content, image treatment, composites, additive manufacturing, Markforged.*

1. Introduction

Additive manufacturing (AM) of continuous fiber-reinforced thermoplastic composites (CFRTPC) using fused deposition modeling (FDM) is a rapidly growing field of research with considerable potential for industrial applications. However, a recent review found a large dispersion of the reported mechanical properties for this kind of material[1]. Such scatter is partially attributed to the uncertainty in fiber volume fraction (*Vf*). Mechanical properties are predicted using models such as the rule of mixtures (ROM) or more advanced models involving homogenization theory, such as asymptotic homogenization. Vignoli et al.[2] have recently reviewed some of them. Melenka et al.[3], and Dutra et al.[4] proposed models for mechanical properties prediction for this specific type of composites. Implementation of numerical models has been done using finite elements for uniaxial direction[5] and uniaxial and transverse directions[4,6]. However, such models consider individual fiber and matrix properties to predict the composite's properties using, at least, the *Vf* as the decisive parameter. Therefore, establishing an accurate *Vf* is one of the key steps to establishing the strength and stiffness of a projected composite material.

Imaging tools are critical to assess the microstructural features of composites[7]. They can serve for damage detection, microstructural determination, and for instance, finding *Vf*, or quality assessment in manufacturing. In damage detection, different authors use SEM, X-ray, and CT to view and correlate damage mechanisms, porosities, and defects with models[8-10]. Quality assessment can be performed through machine vision systems in order to detect major defects in surface roughness, part quality, or warping parts. For the consideration of microstructural analysis via imaging methods, there are different possibilities from Micro CT[11], SEM to Optical microscopy if the fiber diameters are big enough.

For the most part, carbon fiber content is established according to JIS K 7075[12] or ASTM D3171[13] standards, in which a composite part is weighted before being burnt, then, using the known densities, *Vf* is established. However, one must be careful of contents with a high melting temperature, such as calcium carbonates ($CaCO_3$) that might be present in some resins, which may not evaporate, potentially giving an erroneous reading. Furthermore, JIS K 7075[12] is specifically designed for carbon fiber-reinforced composites. In 2008, Cann et al.[14] proposed evaluating *Vf* using image treatment techniques. However, the method posed two problems: first, they counted matrix and fiber areas using a scaling factor to convert pixels to mm, and second, when calculating *Vf*, they kept the area the fiber takes inside the matrix.

Fused deposition modeling is the most widely used AM technology[15,16]. ASTM: F2792 standard defines the AM technique as the process of joining one or more materials to

*e-mail agonzale@uis.edu.co

form objects from 3D topologies, generally layer by layer, as opposed to other manufacturing composite processes. This technology is characterized by having excellent compatibility with different materials, and it allows the construction of highly complex structures.

Moreover, a recent review[1] found the *Vf* for CFRTPC can be confusing to establish. Hence prediction of mechanical properties can be misleading. It has to be noted here the difference between *Vf* and *Vf'* in a composite part. The first one is the fiber content in a spool provided by the supplier, whereas the second is the fiber content in the sample´s cross-sectional area. This means the fiber spool is not made entirely out of fiber. In this work, an approach using digital image techniques is used to extract fiber and matrix area in CFRTPC to calculate an effective *Vf*.

2. Background

2.1. Additive manufacturing

In FDM, a nozzle deposits molten polymer material onto a platform with relative movement, allowing the creation of layers which by continuous and appropriate movements, will reconstruct the CAD topology. If a second nozzle is used for fiber, such as the technology provided by Markforged ®[17], a reinforced polymeric composite can be fabricated.

Figure 1 shows a diagram of the 3D printing process by FDM used by the Markforged Two ® printer. A moving platform is contained within the printing envelope where two extrusion heads, one depositing a matrix polymer (generally Nylon or Nylon-based), and the other deposits continuous fibers (carbon, fiberglass, or Kevlar). The extrusion heads deposit materials layer by layer through their respective nozzles until the sought topology is recreated.

The Markforged Two ® 3D delivers fiber composite materials printed in 3D topologies with strength and elasticity matching aluminum[18], and it can manufacture components with matrix empty space resulting in reduced density parts[19,20].

2.2. Image segmentation

A digital image is a matrix where each position, called a pixel, stores a color value. Depending on the number of bits used, n, one can have 2^N different kinds of gray tones in each pixel, in the case of black and white images[21]. Before an image can be quantitatively analyzed, it needs to be preprocessed to reduce noise and enhance details. Tools like a histogram and the look-up table are used in this stage[22]. Then, segmentation (the process of finding useful information in an image) can be performed. Segmentation methods assign each pixel to a group called a segment. The allocation of a pixel to a particular segment is decided by comparing its gray level to a threshold value[23]. The gray level of a pixel is equivalent to its brightness level, as shown in Equation 1.

$$T = \begin{cases} 0; f(x, y) & < t \\ 1; f(x, y) & > t \end{cases} \quad (1)$$

where T is the threshold, $f(x, y)$ the gray intensity of each pixel, x and y are the Cartesian coordinates of each pixel, and t is the arbitrary gray limit. All the information about other colors is not considered. Since this comparison of values is performed individually for each pixel, the threshold value method is considered a pixel-oriented segmentation method[21]. The output of a filter is obtained by convolution[22]. One can also threshold an image within a range of t. Furthermore, when T is convolved with an image $A(x, y)$, the operation returns a threshold image $B(x, y)$, as described in Equation 2.

$$B[x, y, f(x,y)] = T[x, y] * A[x, y, f(x,y)] \quad (2)$$

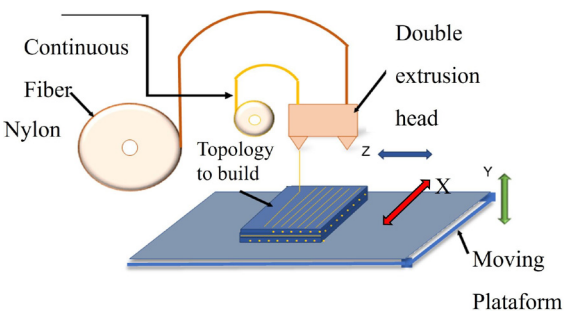

Figure 1. Schematics of FDM printing.

3. Materials and Methods

3.1. Sample preparation

Samples were prepared by cutting about 15 mm unused long carbon, fiberglass, and Kevlar fibers as provided by Markforged ® and placing them in a cylinder filled with epoxy resin until it hardened, as seen in Figure 2a. The top foam shown was used to keep the fibers as vertical as possible while the resin hardened. Then, samples were polished with sandpaper, gradually going from 60 to 2000 grit. After that, samples were gold coated and then placed in a Vega3 Tescan scanning electron microscope (SEM), as shown in Figure 2b, at 10 keV equipped with a tungsten filament. SEM images were taken focusing on each fiber.

3.2. Area counting process

To avoid the pixel to mm scaling, thus, more uncertainty would be introduced in the experiment, two separate pixel counting operations were made: one for the fiber, applying the threshold described in Equation 1, and the convolution of Equation 2, yielding a *Vf* value. The second-pixel counting process was done for the matrix by tracing the matrix perimeter, so the area within could be estimated, namely *Ap*. The process to establish the fiber pixel area is depicted as a flowchart diagram in Figure 3. The general steps taken to preprocess the image and the two individual pixel counting processes can be seen. A similar pixel analysis process has been presented in Lorenzoni et al.[7] for cementious composites, showing an accurate representation of the microstructure. Finally, the method was tested with four 8-bit images from literature.

The *Vf* was calculated by dividing the summation of individual fiber areas, A_f, over the difference between, minus the summation of individual fiber areas, as described in Equation 3. It has to be noted here that the standard *Vf* is calculated as the fiber area ratio over the total area. So, one has to remember the method calculates the *Vf* on the analyzed

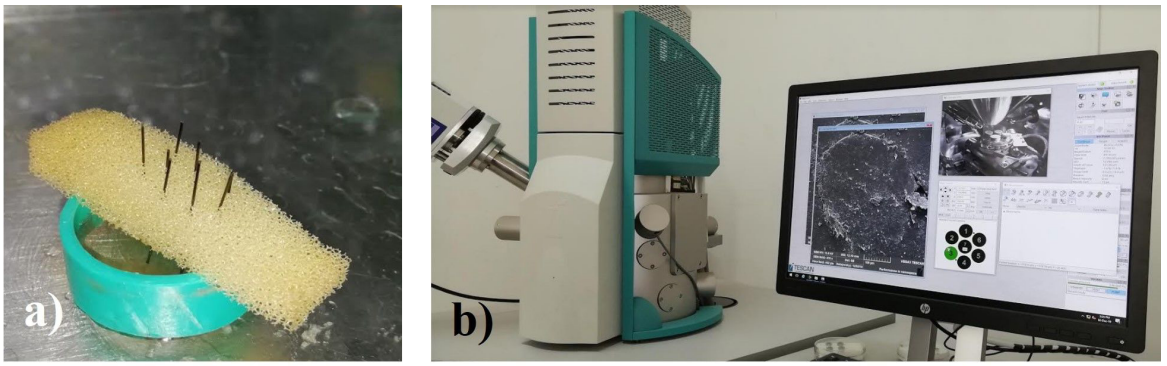

Figure 2. a) fibers solidifying in resin, b) samples mounted in SEM.

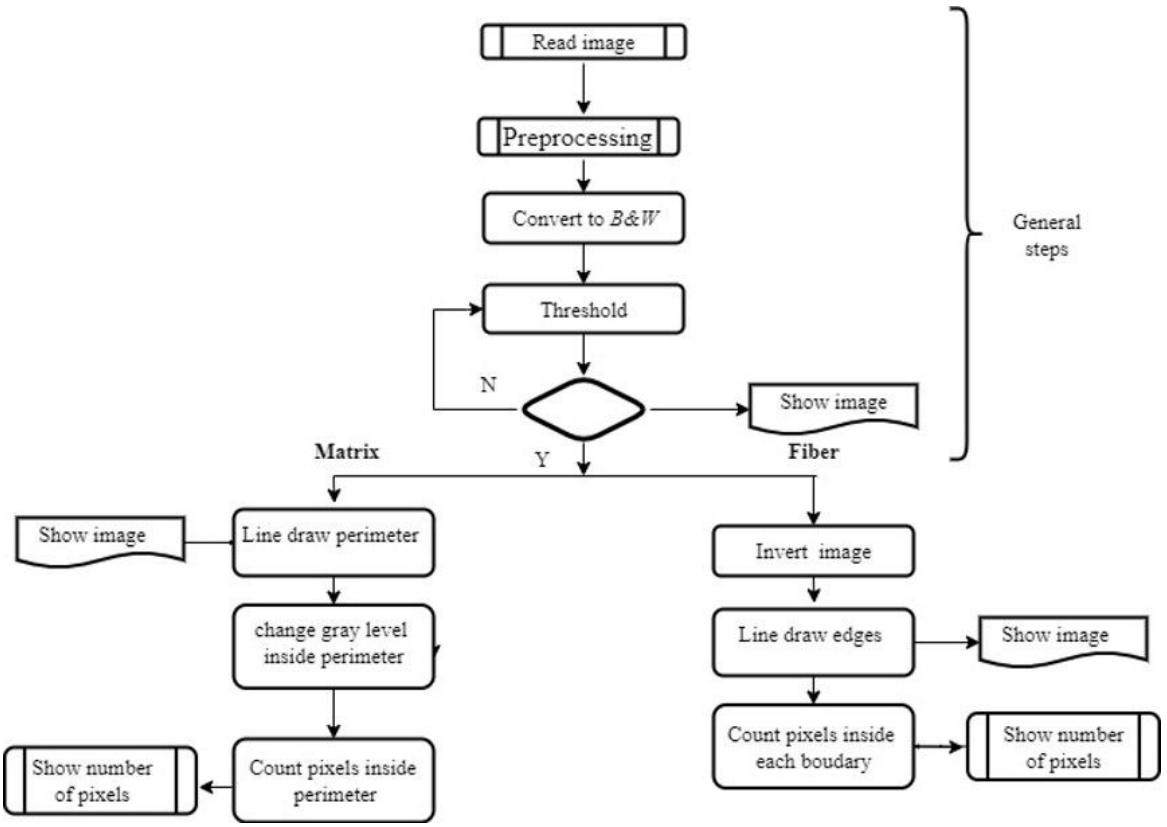

Figure 3. Pixel counting process, including image preprocessing.

section only, not through the part as opposed to the average *Vf* calculated by JIS K 7075.

$$V_f = \frac{A_f}{A_p - A_f} \tag{3}$$

The image processing was performed using *Fiji*[24] for Microsoft Windows ® 64 bits, an enhanced version of *ImageJ* software[25] from the United States National Institutes of Health. *Fiji* runs in Java 1.8 ® or newer and has a public domain license and public source code. As an advantage, *Fiji* can update implemented routines, a handy feature for repetitive tasks. Finally, all images were input in *Fiji* as 8 bit black and white TIFF file format, such that grey values go from 0 to 255, where 0 represents pitch black, and 255 is full light presence.

4. Results and Discussion

A SEM image[26] was used as a benchmark, as shown in Figure 4a, where the fibers are displayed as lighter gray, the matrix and the embedded resin are displayed as a darker gray. The fiber spool, which for now is exclusively provided by Markforged ®, is composed of embedded fibers itself. The fibers, shown as light gray in Figure 4a, are embedded in an Acrylate Scandia Quick® matrix, shown as darker gray in

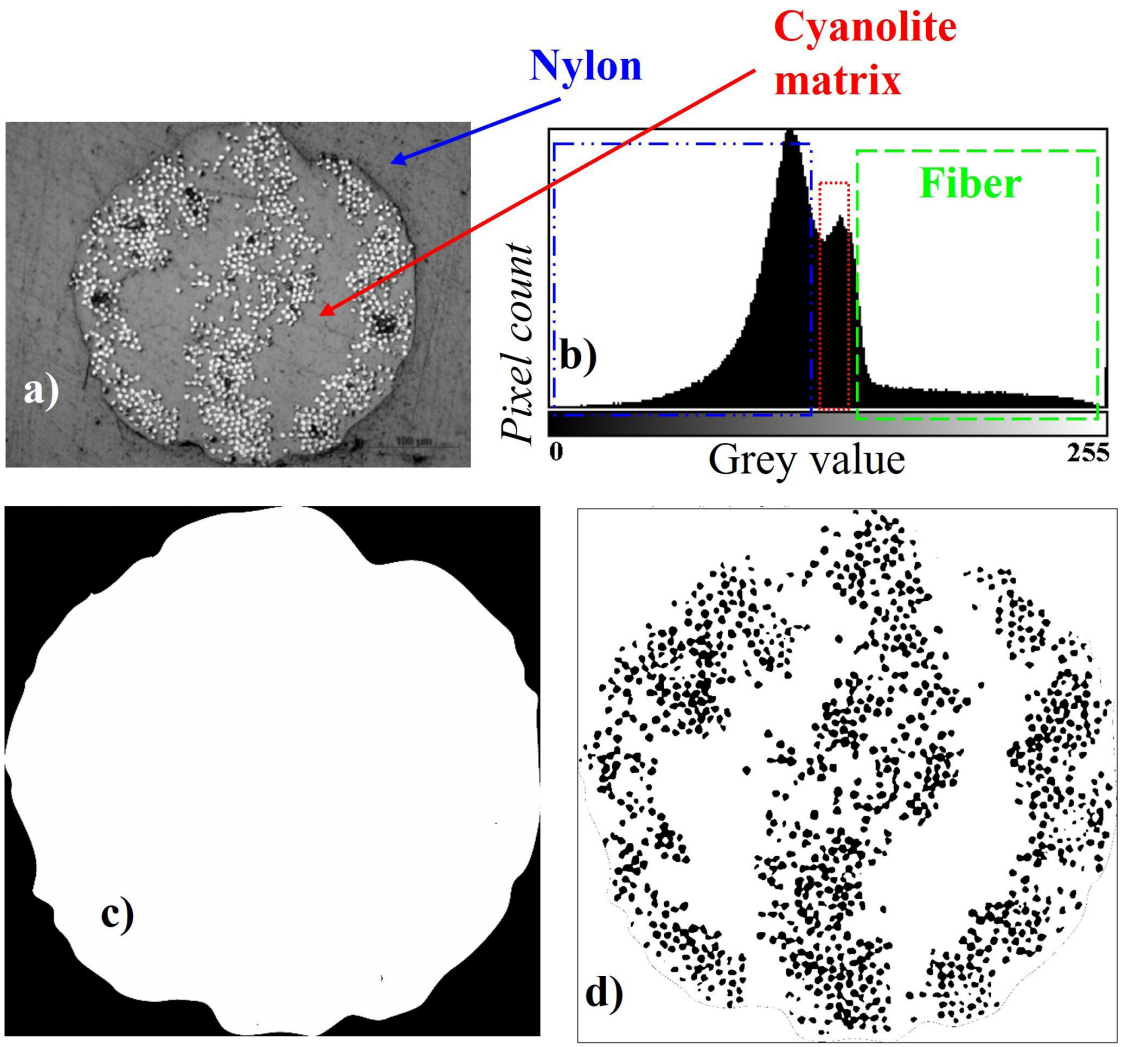

Figure 4. a) Single unprinted carbon fiber bundle showing how fibers are embedded[26], b) histogram showing gray frequency, c) external edge bundle traced, d) lower-limit gray image.

the same figure. Thus, the provided fiber spool is a polymer matrix reinforced with long fibers, making it a composite itself[19]. Figure 4b shows the histogram for Figure 4a, which becomes useful when thresholding the image. A close-up of the carbon bundle cross-section is shown in Figure 4a. The threshold limit can be established by observing the gray image values as shown by Lorenzoni et al.[7]. From the histogram in Figure 4b, one can see that the white areas (single carbon fiber strands) begin to appear at a grey value of about 150. Thus, the threshold level *t* was set at a minimum of 150 and varied until 160; counting the number of pixels with over-the-threshold gray level founding, it kept stable. In the same Figure 4b, the nylon matrix is shown as the darkest grey (about 110 and below) and the cyanolite matrix holding the carbon fibers within the fiber spool peaks at 135.

Following the process described in Figure 3, the total number of pixels was calculated at 6,088,400. Then, the external edge for the bundle was traced, with the outside changed to black, representing a pixel value of 0, and the inside to white, a pixel value of 255, as depicted in Figure 4c. The black area was established as 1,449,193 pixels. Finally, the gray content was thresholded at 150, as shown in the histogram of Figure 4b, with the result shown in Figure 4d. That area count gave 878,351 pixels. Then, Equation 3 gave a *Vf* of 23.35%, which is close to 22.6% reported in[26] for the provided spool *Vf*.

An unused carbon bundle was cut and put under an electronic microscope. The bundle has a nominal diameter between 0.332 and 0.380 mm as reported in[26], and is confirmed as shown in Figure 5.

The embedded-resin carbon fiber bundle is shown in Figure 6a, where one can appreciate the single carbon fibers. The diameter of the single carbon fiber is between 8.55 µm and 8.78 µm, evaluated from Figure 6b, and the single fiber close-up in Figure 6c, values closed to what was reported by Dickson et al.[19]. In addition, the same authors also reported Kevlar fibers sizing 12 µm and fiberglass 10 µm.

Moreover, we performed the same analysis using images 2a and 2d from Chabaud et al.[27]. Due to copyright reasons, the images cannot be displayed. However, Figure 7a and

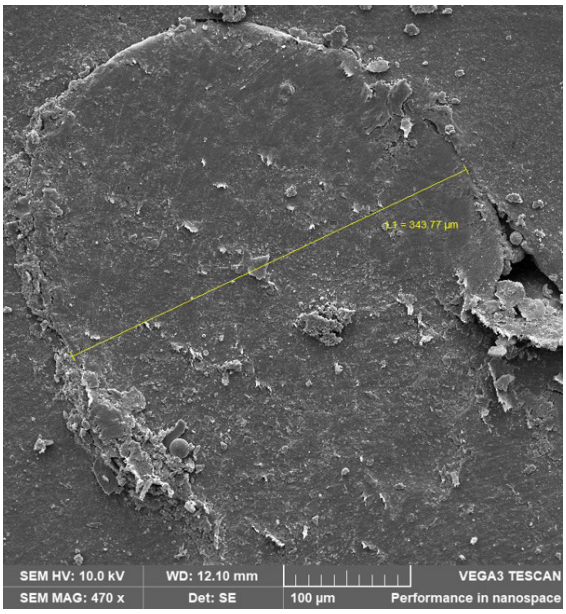

Figure 5. Details of a carbon fiber bundle in SEM micrographs at 470x.

Figure 7b show histograms for images 2a and 2d from Chabaud et al.[27] whereas Table 1 shows the results of pixel counting for said images. On the histograms, one can see the same sudden drop that is observed in Figure 4b; however, in this case, it is more pronounced in Figure 7b. The most significant number of pixels are grouped in one part of the histogram, making it difficult to separate the materials, hence the need for thresholding.

As one can see, the *Vf* is within 1.3% for Image 2d and 1.1% for Image 2a of what Dickson et al.[19] reported. Differences may be attributed to samples not being completely perpendicular to the SEM´s electron beam, to a deviation in threshold choice, or to a difference in voltage potential when taking a picture which can affect gray intensity.

Table 1. Pixel counting for images 2a and 2b from Chabaud et al.[27].

	Image 2a	Image 2d
Fiber pixel area	184,144	213,609
Matrix pixel area	893,328	958,405
Vf	25.97%	28.68%

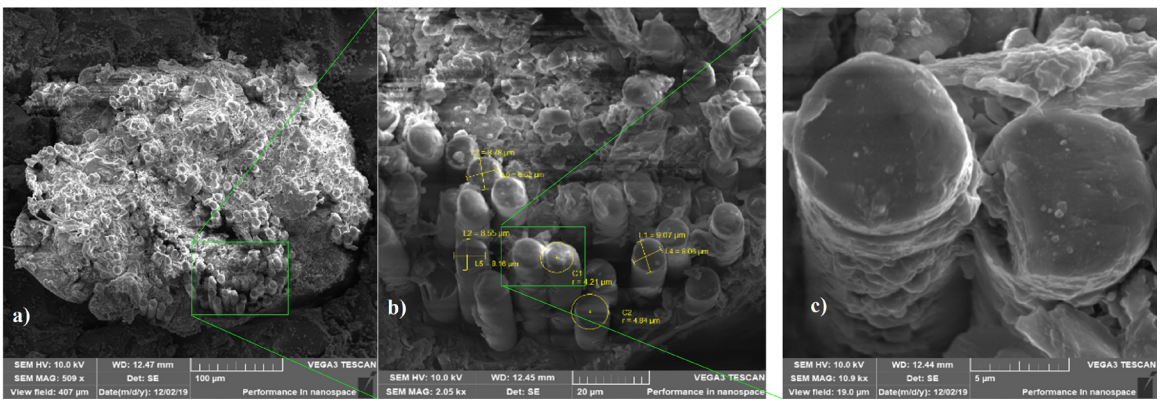

Figure 6. SEM micrographs for: a) embedded carbon fiber bundle at 500x, b) close–up showing individual fibers and measurements at 2.050x, c) single fiber close-up at 2.050x.

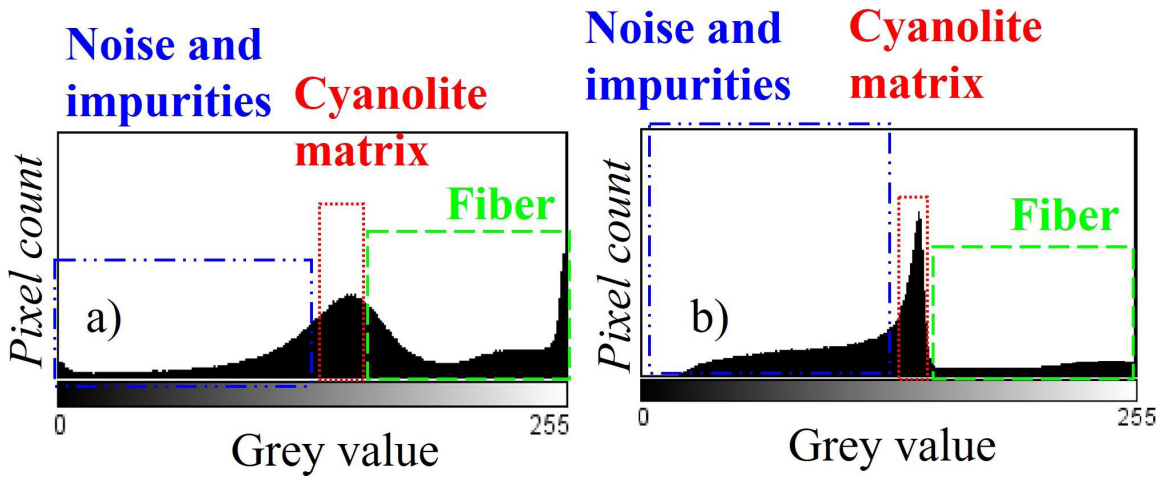

Figure 7. Histograms for figures from Chabaud et al.[27] a) Image 2a and b) Image 2d.

5. Conclusion

Image treatment techniques were used to extract fiber and matrix areas and to obtain the ratio between them. That ratio is called fiber volume fraction, *Vf*. One must not confuse the empty space within the component, which is characteristic of AM, with the matrix inside the fiber bundle, as shown in Figure 6. That empty space in the component is set on purpose in the configuration software to lower the density or due to porosity within consecutive printing head passes. In both cases, they affect mechanical properties, but their effect is calculated with different models. This paper presented a method to calculate the *Vf* within the fiber filaments. It provides an upper bound on the maximum *Vf* obtained by AM process, concerning that some intra-filamentary porosities cannot be removed, and some inter-bead porosities are generated from the manufacturing process.

An initial assessment of gray values should be performed to establish gray values for matrix, fiber, resin, voids, and impurities. After that, one can choose the threshold value. The method was tested with SEM images, but it could be applied to optical images providing there is sufficient magnification, or to 3D images as well. In that case, images from a 3D x-ray tomography can be used, as shown in[28]. The pixel threshold value counting method shows great performance in AM composites, and it could be extended to manufacturing methods and materials.

The proposed method works for CFRTPC. It was tested with a thermoplastic matrix, but when applied to metallic or ceramic matrices, it should work as well. It is an enhancement over existing methods because it does not require calcination. The method calculates the *Vf* in a composite´s cross-sectional area. It is not recommended to be used in short fiber reinforced composites because it only analyzes an area instead of the whole volume, potentially leaving out zones with heterogenous *Vf*. In addition, several cross-section images are recommended because of ovality defects in the filament; not all cross-sections have the same area nor perimeter, implying that local defects such as ovality variations and intra-filamentary porosities could affect the *Vf* value of the cross-section.

When obtaining the images, care should be taken the area is perpendicular to the lens. Failing to do so, e.g., Figure 6a may induce erroneous readings as the pixel counting algorithm might count the lateral fiber surface as transversal fiber area. Also, while this method was used for unprinted filaments, it could be used in printed parts. However, obtaining a valid cross-section for SEM analysis would be a difficult task. The cutting process could result in a damaged cross-section area, altering the *Vf* value evaluation.

6. Acknowledgments

The authors acknowledge financial support from project VIE 2704 2020, at Universidad Industrial de Santander.

7. References

1. Díaz-Rodríguez JG, Pertúz-Comas AD, González-Estrada OA. Mechanical properties for long fibre reinforced fused deposition manufactured composites. Compos, Part B Eng. 2021;211:108657. http://dx.doi.org/10.1016/j.compositesb.2021.108657.
2. Vignoli LL, Savi MA, Pacheco PMCL, Kalamkarov AL. Comparative analysis of micromechanical models for the elastic composite laminae. Compos, Part B Eng. 2019;174:106961. http://dx.doi.org/10.1016/j.compositesb.2019.106961.
3. Melenka GW, Cheung BKO, Schofield JS, Dawson MR, Carey JP. Evaluation and prediction of the tensile properties of continuous fiber-reinforced 3D printed structures. Compos Struct. 2016;153:866-75. http://dx.doi.org/10.1016/j.compstruct.2016.07.018.
4. Dutra TA, Ferreira RTL, Resende HB, Guimarães A. Mechanical characterization and asymptotic homogenization of 3D-printed continuous carbon fiber-reinforced thermoplastic. J Braz Soc Mech Sci Eng. 2019;41(3):1-15. http://dx.doi.org/10.1007/s40430-019-1630-1.
5. Figueiredo JS, Okabe I, Miranda G, Kuwahara M, Fujiyama R, Branco C, et al. Evaluation of the elastic properties of composite materials by the rule of mixtures and computer program. In: 24th COBEM International Congress of Mechanical Engineering; Curitiba. Rio de Janeiro: ABCM; 2017. https://doi.org/10.26678/ABCM.COBEM2017.COB17-2837.
6. Justo J, Távara L, García-Guzmán L, París F. Characterization of 3D printed long fibre reinforced composites. Compos Struct. 2017;185:537-48. http://dx.doi.org/10.1016/j.compstruct.2017.11.052.
7. Lorenzoni R, Curosu I, Paciornik S, Mechtcherine V, Oppermann M, Silva F. Semantic segmentation of the micro-structure of strain-hardening cement-based composites (SHCC) by applying deep learning on micro-computed tomography scans. Cement Concr Compos. 2020;108:103551.
8. Petrò S, Reina C, Moroni G. X-ray CT-Based defect evaluation of continuous CFRP additive manufacturing. Journal of Nondestructive Evaluation. 2021;40(1):7. http://dx.doi.org/10.1007/s10921-020-00737-7.
9. Kastner J, Plank B, Salaberger D, Sekelja J. Defect and porosity determination of fibre reinforced polymers by x-ray computed tomography. In: 2nd International Symposium on NDT in Aerospace 2010 - We.1.A.2; 22-24 Nov 2010; Hamburg, Germany. Germany: NDT in Aerospace; 2010. p. 12.
10. Liu X, Chen F. Defects characterization in CFRP Using X-ray computed tomography. Polym Polymer Compos. 2016;24(2):149-54. http://dx.doi.org/10.1177/096739111602400210.
11. Pinter P, Dietrich S, Bertram B, Kehrer L, Elsner P, Weidenmann KA. Comparison and error estimation of 3D fibre orientation analysis of computed tomography image data for fibre reinforced composites. NDT Int. 2018;95:26-35. http://dx.doi.org/10.1016/j.ndteint.2018.01.001.
12. JIS: Japanese Industrial Standards. JIS K 7075:1991: testing methods for carbon fiber content and void content of carbon fiber reinforced plastics. Japan: JIS; 1991.
13. ASTM: American Society for Testing and Materials. ASTM D3171: standard test method for constituent content of composite materials. West Conshohocken: ASTM; 2015. https://doi.org/10.1520/D3171-15.
14. Cann MT, Adams DO, Schneider CL. Characterization of fiber volume fraction gradients in composite laminates. J Compos Mater. 2008;42(5):447-66. http://dx.doi.org/10.1177/0021998307086206.
15. León-Becerra J, González-Estrada OA, Quiroga J. Effect of relative density in in-plane mechanical properties of common 3D-printed polylactic acid lattice structures. ACS Omega. 2021;6(44):29830-8. http://dx.doi.org/10.1021/acsomega.1c04295.
16. León BJ, Díaz-Rodríguez JG, González-Estrada OA. Daño en partes de manufactura aditiva reforzadas por fibras continuas. Revista UIS Ingenierías. 2020;19(2):161-75. http://dx.doi.org/10.18273/revuin.v19n2-2020018.
17. Mark GT, Gozdz AS. Three dimensional printer with composite filament fabrication. United States Patent US10226103. 2015.
18. González-Estrada OA, Pertuz Comas AD, Díaz Rodríguez JG. Monotonic load datasets for additively manufactured

thermoplastic reinforced composites. Data Brief. 2020;29:4-6. http://dx.doi.org/10.1016/j.dib.2020.105295.

19. Dickson AN, Barry JN, McDonnell KA, Dowling DP. Fabrication of continuous carbon, glass and Kevlar fibre reinforced polymer composites using additive manufacturing. Additive Manufacturing. 2017;16:146-52. http://dx.doi.org/10.1016/j.addma.2017.06.004.
20. Pertuz AD, Díaz-Cardona S, González-Estrada OA. Static and fatigue behaviour of continuous fibre reinforced thermoplastic composites manufactured by fused deposition modelling technique. Int J Fatigue. 2020;130:105275. http://dx.doi.org/10.1016/j.ijfatigue.2019.105275.
21. Gonzalez RC, Woods RE. *Digital image processing.* 3rd ed. Harlow: Pearson Education; 2008.
22. Paciornik S, Mauricio MHP. *Digital imaging.* 1st ed. Rio de Janeriro: PUC-RJ; 2016.
23. Díaz JG, Paez DC. (2021). Identification of crack tip location using edge detection algorithms and artificially generated displacement fields. In: Cortes Tobar D, Hoang Duy V, Trong Dao T, editors. *AETA 2019 - Recent Advances in Electrical Engineering and Related Sciences: theory and application*. Springer, Cham. (Lecture Notes in Electrical Engineering, Vol 685).
24. Rueden CT, Schindelin J, Hiner MC, DeZonia BE, Walter AE, Arena ET, et al. ImageJ2: ImageJ for the next generation of scientific image data. BMC Bioinformatics. 2017;18:671-5. http://dx.doi.org/10.1186/s12859-017-1934-z.
25. Abramoff MD, Magalhaes PJ, Ram SJ. Image processing with ImageJ. Biophoton Int. 2004;11(7):36-42.
26. Blok LG, Longana ML, Yu H, Woods BKS. An investigation into 3D printing of fibre reinforced thermoplastic composites. Additive Manufacturing. 2018;22:176-86. http://dx.doi.org/10.1016/j.addma.2018.04.039.
27. Chabaud G, Castro M, Denoual C, le Duigou A. Hygromechanical properties of 3D printed continuous carbon and glass fibre reinforced polyamide composite for outdoor structural applications. Additive Manufacturing. 2019;26:94-105. http://dx.doi.org/10.1016/j.addma.2019.01.005.
28. Stamati O, Roubin E, Andò E, Malecot Y, Charrier P. Fracturing process of micro-concrete under uniaxial and triaxial compression: insights from in-situ X-ray mechanical tests. Cement Concr Res. 2021;149:106578.